BILINGUAL PUBLISHING CO.
Pioneer of Global Academics Since 1984

Journal of Metallic Material Research
http://ojs.bilpublishing.com/index.php/jmmr/manager

REVIEW

Combined Effect of Thermal Shock and Hot Corrosion on the Failure of Yttria Stabilized Zirconia Thermal Barrier Coatings

Changhai Zhou* XueWei Li Ruiyun Pan

School of Materials Science and Engineering, Heilongjiang University of Science and Technology, 2468 Pu-Yuan Road, Harbin 150022, P. R. China

ARTICLE INFO

Article history:
Received: 9 November 2018
Accepted: 28 December 2018
Published: 31 December 2018

Keywords:
Thermal barrier coatings
Hot corrosion
Thermal shock
Failure

ABSTRACT

The application of thermal barrier coatings (TBCs) always undergo severe environment, concluding hot corrosion, high temperature oxidation and high stress, which result in the failure of TBCs. The study of failure mechanisms of TBCs under various combined environmental factors, different with single factor, is more significant to further promote the applications of TBCs. In the present work, the combined effect of thermal shock and hot corrosion on the failure of TBCs was highlighted investigated. The 8wt.% yttria stabilized zirconia (8YSZ) thermal barrier coatings on a GH4132 alloy were deposited by air plasma spraying. The results showed that the transformation of ZrO2 from tetragonal phase to monoclinic phase induced internal stress in the topcoat when combined with the thermal stress, the topcoat even the bondcoat were both cracked. The main failure of TBCs under the combined effect was in the form of penetrating crack to the bondcoat/substrate interface and oxidation at the penetrating crack front.

1. Introduction

Thermal barrier coatings are applied in gas turbines owing to their effective thermal insulation to the hot section components[1,2]. Typical TBCs consist of partially stabilized zirconia topcoat for thermal insulation layer and a metallic bondcoat for oxidation/corrosion resistant and thermal stress relaxation[3-5]. So far, materials, depositing technology and properties of the thermal barrier coatings have been intensively investigated[3-19]. During these studies, the failure of TBCs is a core evaluation for various materials and depositing technologies. Commonly, thermal cycling and hot corrosion tests, simulating the operating conditions of the TBCs, are carried out to explore the failure of TBCs [20-35]. During thermal cycling, the YSZ coatings are stressed because of the mismatching of thermal expansion coefficients between topcoat and metallic bond coat. When the stress is accumulated to a critical value, the TBCs finally fails[2,12-15,20-26]. For hot corrosion of the TBCs, a mixture salt containing vanadate and sulfate is used to study the failure mechanism of the TBCs. It is conducted that the stabilizer of Y_2O_3 reacts with corrosive salt, reducing the stability of ZrO_2, and therefore inducing the phase transformation of tetragonal to monoclinic [27-35]. Those phase transformations, accompanied with 3~5% volume change, can cause the failure of the TBCs[1,29,35,36]. In the previous investiga-

**Corresponding Author:*
Changhai Zhou
School of Materials Science and Engineering, Heilongjiang University of Science and Technology,
2468 *Pu-Yuan Road, Harbin* 150022*, P. R. China*
*Email: dlut*2325@163*.com*

 DOI: https://doi.org/10.30564/jmmr.v1i1.307

tions, the thermal shock and hot corrosion behaviors of the TBCs are studied independently. The combined effect of them on the failure of the TBCs is seldom. Application environments of the TBCs, however, are always simultaneously accompanied with hot corrosion and thermal shock, such as turbine blades. Then, failure of TBCs under such combined environment would be complicated. The failure mechanism of TBCs needs to investigate deeply. In this work, the thermal shock, hot corrosion and the combined tests of the TBCs on a GH2132 alloy were carried out, and the combined effect of thermal shock and hot corrosion on the failure of the TBCs was highlighted investigated.

2. Experimental Procedure

2.1 Materials and Coating Preparation

A GH2132 (Fe-25Ni-15Cr) alloy was used as the substrates with dimensions of 20mm × 20mm × 2mm. TBCs composed of a ceramic topcoat (8wt.% Y_2O_3 stabilized ZrO_2) and a bond coat (Ni23Co20Cr8.5Al1Y) were deposited on the substrate alloy with the air plasma spray (APS) process. Prior to spraying process, the substrates were grit blasted by SiC particles with the size of 90μm in order to increase the surface roughness to strengthen the sprayed coating adhesion. They were then cleaned with absolute ethyl alcohol in an ultrasonic set and preheated with plasma gun before spraying. Subsequently, an air plasma spray (APS) system (Switzerland PT Corporation, R-750C) was used for overlaying the NiCoCrAlY bond coat and YSZ topcoat on the substrates. Table 1 displays the spraying parameters.

Table 1. Processing parameters for spraying coatings

parameter	coat	bond coat
Current (A)	5	450
Voltage (V)	60	55
Primary gas, Ar (l/min)	40	50
Secondary gas, H_2 (l/min)	8	12
Powder feed rate (g/min)	20	30
Spray distance (cm)	10	15

2.2 Thermal Shock and Hot Corrosion Tests

The thermal shock test was carried out in a muffle furnace. When the temperature of the furnace reached up to 900 ℃ , the specimens were pushed into the furnace, and held about 15 min. They were then directly quenched into the air. After about 2 min, the temperature of specimens reached the room temperature.

The hot corrosion tests were also conducted in a muffle furnace. The corrosive salt was a mixture of 50wt.% Na_2SO_4 and 50wt.% V_2O_5 powders. And the corrosive salt was strewed over the coating surface in a concentration of 2 mg/cm^2. The specimens were pushed into the muffle furnace at 900 ℃ for 10 h and 40 h, respectively, and then cooled down inside the furnace in order to prevent the phase transformation from the fast cooling.

In order to investigate the combined effect of thermal shock and hot corrosion of the TBCs, a test including thermal shock and hot corrosion was designed. Prior to the test, the surface of coatings was strewed by corrosive salt with a concentration of 2 mg/cm^2. Then, the thermal shock tests of the specimens with corrosive salt were carried out. This test was defined as thermal-cycle corrosion.

2.3 Characterization

The morphologies including top view and cross-sections of TBCs before/after the thermal shock and hot corrosion tests were examined by scanning electron microscopy (SEM). As well X-ray diffraction operating with Cu-K_α radiation was used to determine the phase composition of coatings and the corrosion products.

3. Results

3.1 Characterization of As-sprayed Coatings

Fig. 1 shows the surface, cross-sectional morphologies and XRD patterns of the as-sprayed TBCs. Pores, microcracks, splat boundaries and occasional unmelted particles were seen on the surface of coating. These defects are regarded as the common characteristics of APS ceramic coatings[1,2,9,15,20]. The topcoat displays a characteristic lamellar structure composed by mechanically interlocking molten splats and high micro-scaled porosities. Because of the less plastic deformation upon collision with bondcoat surface, the topcoat shows low density of YSZ[1,2]. The XRD pattern of the as-sprayed coatings, Fig. 1(c), implies that it was only nonequivalent tetragonal phase (t'-ZrO_2) in the coatings. It is well known that the content of Y_2O_3 and the cooling rate are the key factors on the formation of t'-ZrO_2 [36,37]. It can ensure the stabilization of ZrO_2 for the content of 8wt% Y_2O_3 used in the present work. However, the diffusionless transformation to form t-ZrO_2 occurred due to the quenching effect of the high cooling rate during spraying [37].

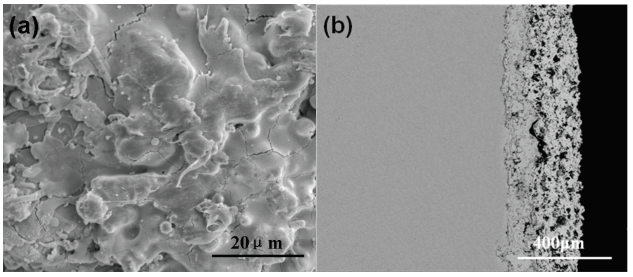

DOI: https://doi.org/10.30564/jmmr.v1i1.307

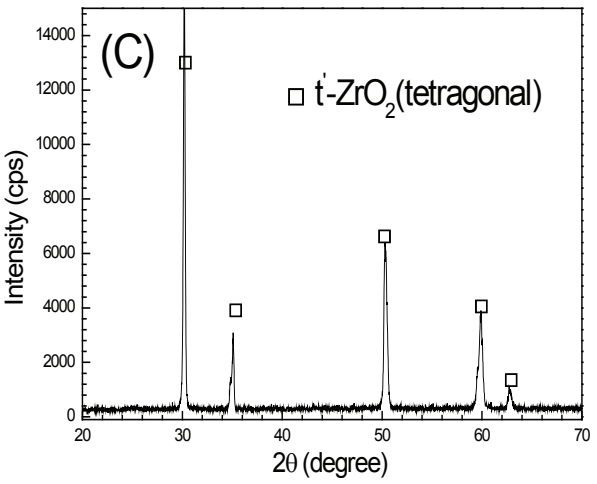

Figure 1. Morphologies and phase composition of the as-sprayed coatings (a) surface morphology; (b) cross-sectional morphology; (c) XRD pattern

3.2 The Surface Morphologies of TBCs after Thermal Shock Test

Figure 2 shows surface morphologies of the TBCs after the thermal shock and thermal-cycle corrosion tests. As can be seen in Fig.2(a), only a few cracks formed on the topcoat surface after 40-cycle thermal shock test. However, in the case of 40-cycle thermal corrosion test, obvious cracks generated and presented latticed morphology. It is implied that the corroded effect would increase the cracking tendency of the TBCs. Though the topcoat of TBCs cracked after 150-cycle thermal shock test, the number and density of cracks are still lower than that after 40 thermal-cycle corrosion test and far below than that after 150 thermal-cycle corrosion test, as shown in Fig. 2. It is further confirmed that the combined effect of thermal shock and hot corrosion could accelerate the failure of TBCs.

3.3 The Surface Morphologies of TBCs after Hot Corrosion Test

Fig. 3 displays the surface morphologies of TBCs after hot corrosion and thermal-cycle corrosion tests. As can be seen in Fig.3(a), needle-shaped corrosion products have been formed on the coating surface after 40 thermal-cycle corrosion tests. Obvious cracks were also developed in the surface coating owing to the effect of thermal shock. Besides, some needle-shaped corrosion products seemed to nucleate in those cracks and outward grow. Meanwhile, some lath-shaped corrosion products formed in those cracks. However, only rod-shaped corrosion products formed on the coating surface after 10 h of corrosion (the corrosion time is equal to that of 40 thermal-cycle effective corrosion time). It is implied that the combined effect

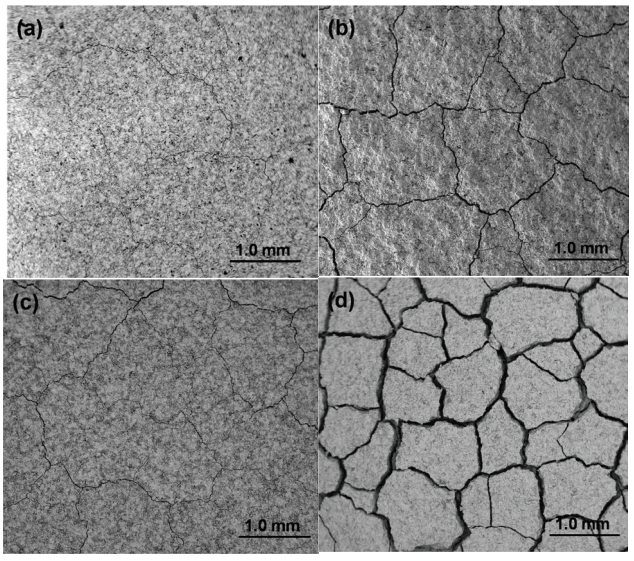

Figure 2. Surface morphologies of 8YSZ thermal barrier coating after (a) 40-cycle thermal shock test; (b) 40 thermal-cycle corrosion test; (c) 150-cycle thermal shock test; (d) 150 thermal-cycle corrosion test

of thermal shock and hot corrosion changed the morphologies of corrosion products. With the increase in corrosion time, obvious bundle-shaped and laminate-shaped corrosion products were embedded in the coating after 150 thermal-cycle corrosion tests (the effective corrosion time is equal to 40 h). Pores still existed in the coatings and in where corrosion products formed. In the case of hot corrosion, long dendritic corrosion products formed on the coating surface.

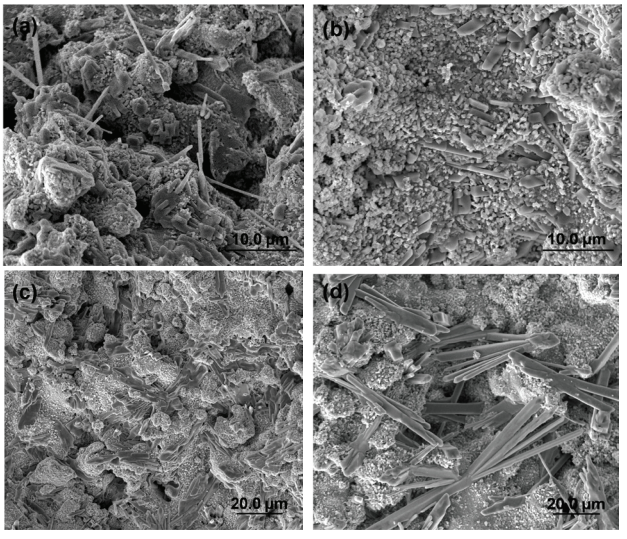

Figure 3. Surface morphologies of TBCs after (a) 40 thermal-cycle corrosion test; (b) 10 h of hot corrosion test; (c) 150 thermal-cycle corrosion test; (d) 40 h of hot corrosion test

Fig. 4 shows the XRD patterns of TBCs after hot corrosion and thermal-cycle corrosion tests for effective cor-

rosive time of 10 h and 40 h. As can be seen, most of the tetragonal zirconia in the YSZ had changed to the monoclinic phase and yttrium vanadate formed as hot corrosion products.

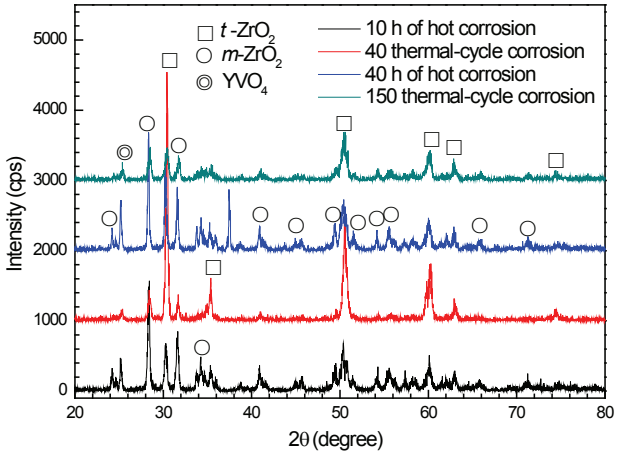

Figure 4. XRD patterns of 8YSZ thermal barrier coatings after corrosion

3.4 The Cross-sectional Morphologies of TBCs after Thermal Shock Test

Fig. 5 presents SEM micrographs of cross sections of the coatings after thermal shock and thermal-cycle corrosion tests. According to the micrographs, no obvious cracks generated after 40-cycle thermal shock. However, obvious vertical and even penetrating cracks occurred after 40 thermal-cycle corrosion tests. After 150-cycle thermal shock, vertical and penetrating cracks generated. And the penetrating cracks widened under the corrosive conditions. Besides, oxide formed at the tip of the penetrating cracks. It can be gained that the failure is inevitable for the TBCs during thermal shock owing to the nature of TBCs themselves, but the additional corrosive condition accelerates the failure progress.

4. Discussion

4.1 Effect of Thermal Shock on the Failure of TBCs

Based on the aforementioned results, TBCs are prone to failure under the combined thermal shock and hot corrosion conditions and whose failure mechanism is different with that of individual thermal shock and hot corrosion. Under the hot shock condition, the failure of TBCs is mainly based on the accumulated thermal stress arose from the mismatch of thermal expansion coefficient between topcoat, bond coat and substrate[2,12,20-26]. When the thermal stress reaches the critical value, the vertical and horizontal cracks are initially generated according to the local stress status of the coatings. After that, the cracks

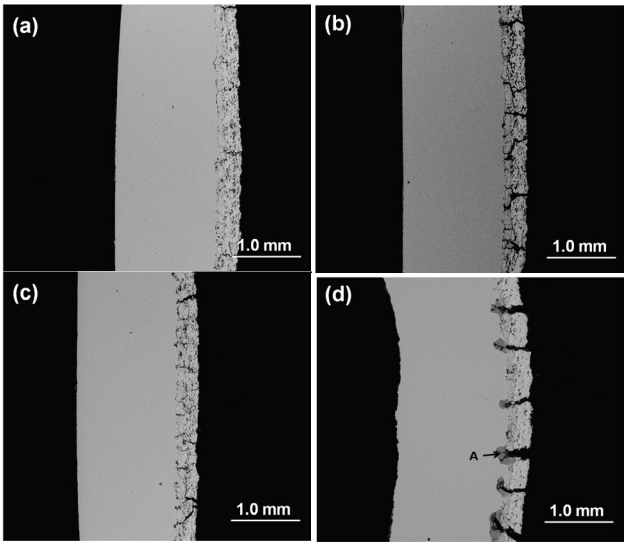

Figure 5. Cross-sectional morphologies of 8YSZ thermal barrier coatings under the conditions of (a) 40-cycle thermal shock; (b) 40 thermal-cycle corrosion; (c) 150-cycle thermal shock; (d) 150 thermal-cycle corrosion

propagate and finally result in the failure of TBCs [2,12, 26]. In the present work, no obvious cracks formed after 40-cycle thermal shock owing to the fact that the accumulated thermal stress is lower than the critical stress to form initial crack. Up to 150-cycle thermal shock test, typical cracking failure of TBCs on the Fe-based alloy was observed [25]. The cracking failure mainly contained penetrating cracks from topcoat to the topcoat/bond coat and bond coat/substrate interface, linked horizontal cracks and short vertical cracks near the surface of topcoat.

4.2 Effect of Hot Corrosion on the Failure of TBCs

Hot corrosion behavior of thermal barrier coatings in the mixture of vanadium and sulfur salt has been intensively investigated [26-37]. The main mechanism is the dissolution of YSZ thermal barrier coatings in the molten salt by re-precipitation of both yttrium vanadate and yttrium depleted monoclinic zirconia. According to the previous studies and the present work, the hot corrosion behavior can be elaborated as the following reactions[28,31-35]:

$$V_2O_5 + Na_2SO_4 \rightarrow 2NaVO_3 + SO_3 \quad (1)$$

$$ZrO_2\,(Y_2O_3) + 2NaVO_3 \rightarrow ZrO_2\,(\text{monoclinic}) + 2YVO_4 + Na_2O \quad (2)$$

During the hot corrosion process, the mixture of molten salts firstly reacted with each other and formed $NaVO_3$, as reaction 1. Then, $NaVO_3$ will react with stabilizer component of Y_2O_3 in topcoat to form YVO_4, monoclinic ZrO_2 and Na_2O. Also, the formed Na_2O can react with V_2O_5 directly to form $NaVO_3$, as reaction 3[29,31].

$$Na_2O + V_2O_5 \rightarrow 2NaVO_3 \quad (3)$$

Some studies[28,33], with regard to YSZ hot corrosion,

DOI: https://doi.org/10.30564/jmmr.v1i1.307

reported that Y_2O_3 in topcoat reacted directly with V_2O_5 to form YVO_4 by the following reaction:

$$ZrO_2\ (Y_2O_3) + V_2O_5 \rightarrow ZrO_2\ (\text{monoclinic}) + 2YVO_4 \quad (4)$$

With regard to other possible chemical reaction about the YSZ corrosion in vanadium and sulfur molten salt, the following reaction can be given [30].

$$ZrO_2 + V_2O_5 \rightarrow ZrV_2O_7 \quad (5)$$

However, XRD patterns in Fig.4 showed that the reaction products of ZrV_2O_7 could not be detected. One side, the reaction is so low and seldom detected [29,35]. On the other side, ZrV_2O_7 is easy to transform to ZrO_2 and V_2O_5 above 750℃ [30,38]. Therefore, no corrosion product of ZrV_2O_7 was found in this work.

Above corrosion process of YSZ in sulfate and vanadate molten salt is widely used to analyze the hot corrosion behavior of the YSZ coating. However, it is changed for that hot corrosion behavior under thermal shock condition. Especially, the content of monoclinic phase of hot corrosion is different with that of thermal-cycle corrosion. The volume fractions of the monoclinic phase, as the criteria for YSZ coatings destabilization during hot corrosion test, are calculated by the following equation based on the calculation of the peak intensity ratio[28,32,34,35].

$$m\% = \frac{I_m(\bar{1}11) + I_m(111)}{I_m(\bar{1}11) + I_m(111) + I_t(111)} \times 100\% \quad (6)$$

where, I_m is the intensity of monoclinic peaks, It is the intensity of tetragonal peaks. It can be gained that the content of the monoclinic phase is 40.8% for 1 h of corrosion and decreasing to 31.6% for 40 h of hot corrosion. The decrease of that is due to the fact that the formation of long dendritic corrosion products not only cover the coating surface but also increase the stress inducing the m-ZrO_2 spall from the coating. Therefore, detected content of monoclinic phase by the XRD was somewhat decreased with the increasing of the time. In the case of thermal-cycle corrosion, the contents of monoclinic phase are 18.1% and 34.8% after 40 and 150 thermal-cycle corrosion, respectively. It can be seen that these contents are lower than those under hot corrosion. This is because that the coating surface simultaneously undergoes the thermal stress and phase-transformation stress during the thermal-cycle corrosion. The m-ZrO_2 and the formed corrosion products would spall from the coating surface. After 40 thermal-cycle corrosion, the needle-liked corrosion products showed poor bond force to the coating and were prone to spalling. At the same time, that process induces some local YSZ spall from the coating surface. As a result, the content of monoclinic phase was so low. With the growth of corrosion products, they were embedded in the coating. The trend of spallation was decreased. The continued and steady growth of corrosion products consumes the yttria. The relative transformation of t-ZrO_2 to m-ZrO_2 occurs. Therefore, the content of monoclinic phase is increased. Moreover, the XRD patterns of TBCs after thermal shock tests were detected, as shown in Fig. 6. As can be seen, after 40-cycle thermal shock test, zirconia was present only in the tetragonal phase. This implies that no destabilization occurred in the coatings. Even after 150-cycle thermal shock, it was still no monoclinic phase to form. It is verified that the transformation from tetragonal ZrO_2 to monoclinic ZrO_2 during the thermal-cycle corrosion is only attributed to the hot corrosion process of YSZ. Then, it could be proposed that the final failure of TBCs under the thermal-cycle corrosion condition should be the result of thermal stress and the stress resulted from the volume changes of ZrO_2 induced by hot corrosion. In another word, the failure of TBCs is attributed to the strained condition during the test.

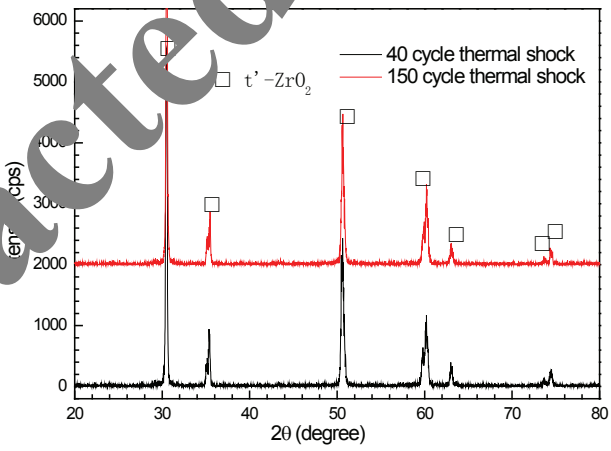

Figure 6. XRD patterns of TBCs after thermal shock tests

4.3 Failure Analyses of TBCs under the Combined Effect of Hot Corrosion and Thermal Shock

The strain tolerance of TBCs is clearly analyzed from the stress–strain curve of ceramic coatings [39]. And, the strain for the TBCs is nonlinear and can be expressed by [40]:

$$\varepsilon = \varepsilon^e + \varepsilon^{ne} \quad (7)$$

where ε^e represents

$$\varepsilon^e = \frac{\sigma}{E} \quad (8)$$

which is the nominal strain and is estimated on the basis of linear elastic behavior, and where ε^{ne} represents the inelastic strain resulting from laminar and microcrack structures. The thermal expansion mismatch of topcoat, bond coat and substrate would lead to stressing forming during the thermal shock tests. Though the thermal stress cannot change the linear elastic behavior of a TBC, it can

affect the inelastic strain of TBCs in the form of inducing the microcrack forming. During the thermal-cycle corrosion test, not only the thermal stress but also the stress from the volume change owing to ZrO_2 phase transformation will rapidly accumulate to a critical value to induce initial crack forming after a certain thermal cycle. Then the inelastic strain tolerance related to the laminar and microcrack structures would reduce. And the strain tolerance of TBCs would also reduce according to equation (7), even the TBCs lose the strain tolerance and occur to spall in the end. A failure model of TBCs under the combined effect of hot corrosion and thermal shock was proposed, as shown in Fig. 7. During initial thermal-cycle corrosion, the accumulated thermal stress is so small that cannot induce the crack forming of TBCs, but the hot corrosion can induce an additional stress to the topcoat. As a result, the initial microcracks form near the surface of topcoat, as Fig. 7(b) shown. With the increasing of thermal cycles and further hot corrosion, the stress in the topcoat will increase and some initial cracks begin to inward expand and widen, as Fig. 7(c) indicated. After that, penetrating cracks are inevitable developed due to the thermal expansion mismatch difference between bond coat and substrate. Then oxygen and corrosive salt transport to the tips of these penetrating cracks, and reacts with the substrate there, shown in Fig. 7(d). These oxidation/corrosion products in Fig.5(d) pointed by A were examined by EDS, as shown in Fig. 8. It can be seen that these products only comprise O, Cr, Fe and Ni elements, which indicates the substrate of GH2132 alloy oxidized with oxygen. After

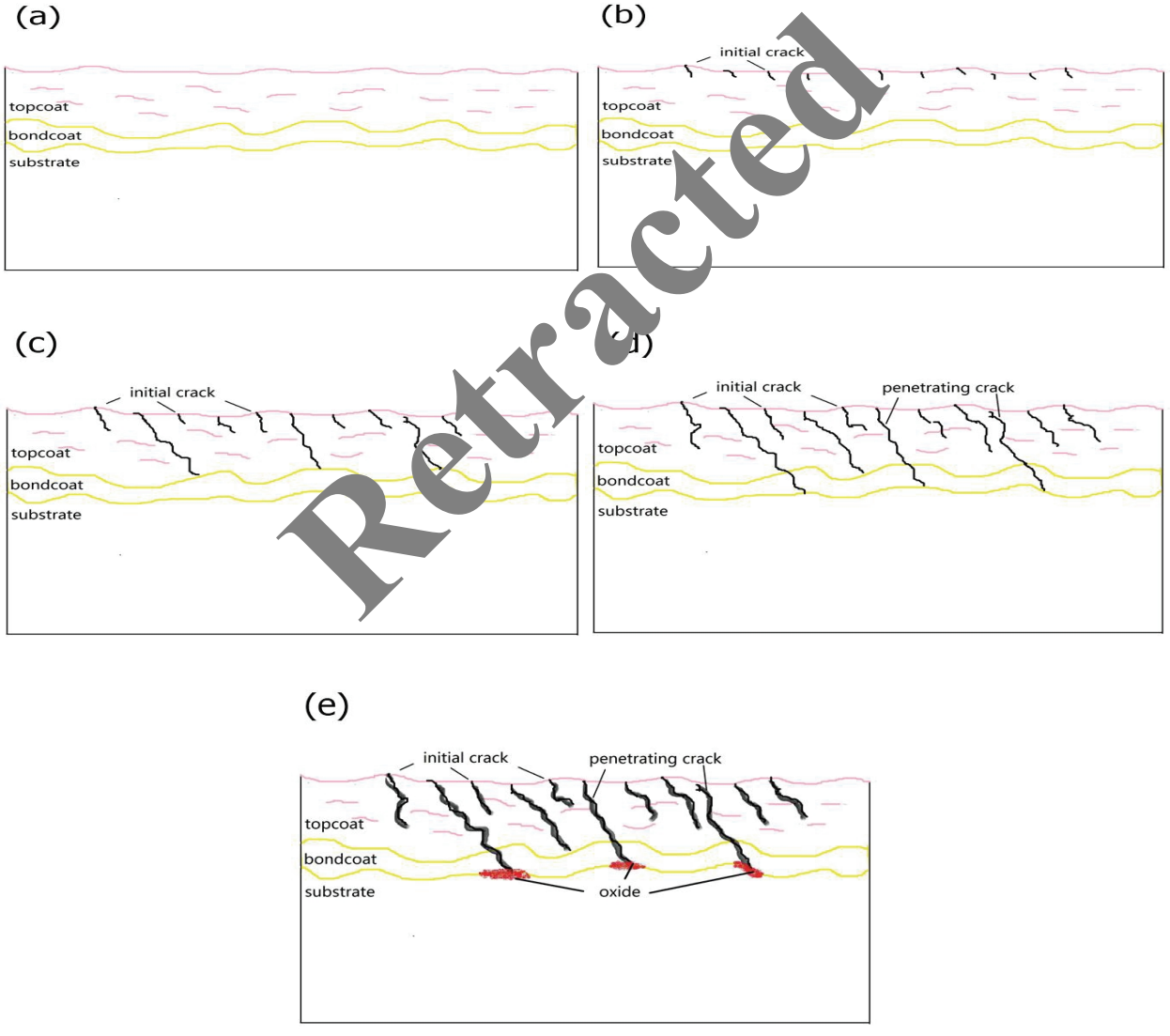

Figure 7. The failure process of TBCs under the combined effect of hot corrosion and thermal shock (a) as-sprayed coating; (b) initial microcrack forming in topcoat; (c) microcrack inward expanding; (d) penetrating crack forming; (e) oxide forming at the bondcoat/substrate interface

DOI: https://doi.org/10.30564/jmmr.v1i1.307

that, a lateral growth of the oxide along the bond coat and substrate interface occurred to form local oxidation zone. With the thermal cycle further increasing, the penetrating cracks widen and new microcracks occur to form in topcoat, and finally the TBCs would separate from the substrate to lose its protection.

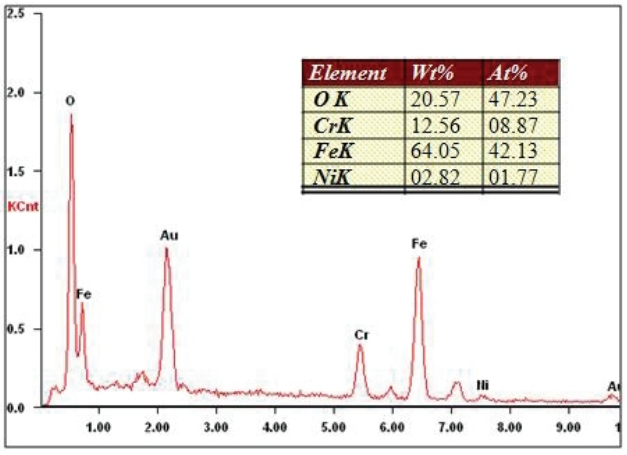

Figure 8. EDS analysis of oxide pointed by A in Fig. 5(d)

5. Conclusions

The thermal shock, hot corrosion and thermal-cycle corrosion tests of 8wt.% yttria stabilized zirconia prepared by air plasma spraying were carried out at 900℃ . The combined effect of thermal shock and hot corrosion on the failure of TBCs was investigated, the main conclusion as follows:

1) Compared with thermal shock of TBCs, the initial cracks was more ealier formed in topcoat during the thermal-cycle corrosion due to the induced stress of transformation of ZrO2.

2) The main failure of TBCs under the combined effect was penetrating cracks to the bond coat and substrate interface and oxidation at the tips of the penetrating cracks.

Acknowledgments:The work was financially supported by the National Natural Science Foundation of China (NSFC, Grant No. 51501058).

References

[1] R.A. Miller, Current status of thermal barrier coatings: an overview, Surf. Coat. Technol. doi.org/10.1016/0257-8972(87)90003-X

[2] N.P. Padture, M. Gell, E.H. Jordan, Thermal Barrier Coatings for Gas-Turbine Engine Applications, Science .doi:10.1126/science.1068609

[3] X.Q. Cao, R. Vassen, D. Stoeve, Ceramic materials for thermal barrier coatings, J. Eur. Ceram. Soc. doi. org/10.1016/S0955-2219(03)00129-8

[4] C.G. Levi, Emerging materials and processes for thermal barrier systems, Curr. Opin. Solid State Mater. Sci. doi. org/10.1016/j.cossms.2004.03.009

[5] R. Vassen, X.Q. Cao, F. Tietz, D. Basu, and D. Stover, Zirconates as New Materials for Thermal Barrier Coatings, J. Am. Ceram. Soc. doi:10.1111/j.1151-2916.2000.tb01506.x

[6] D.R. Clarke and C.G. Levi, Materials Design for the Next Generation Thermal Barrier Coatings, Annu. Rev. Mater. Res. doi:10.1146/annurev.matsci.33.011403.113718

[7] C.U. Hardwicke, Y.C. Lau, Advances in Thermal Spray Coatings for Gas Turbine and Energy Generation: A Review, J. Therm. Spray Technol. doi:10.1007/s11666-013-9904-0

[8] G. Sivakumar, S. Banerjee, S. Raja, S.V. Joshic, Hot corrosion behavior of plasma sprayed powder-solution precursor hybrid thermal barrier coatings, Surf. Coat. Technol. doi.org/10.1016/j.surfcoat.2018.06.021

[9] D. Stöver, G. Pracht, H. Lehmann, M. Dietrich, J-E. Döring, and R. Vaßen, New Material Concepts for the Next Generation of Plasma-Sprayed Thermal Barrier Coatings, J. Therm. Spray Technol. doi:10.1007/s11666-004-0052-4

[10] J. Karthikeyan, C.C. Berndt, S. Reddy, J.Y. Wang, A.H. Kumar, and C. Herman, Nanomaterial Deposits Formed by DC Plasma Spraying of Liquid Feedstocks, J. Am. Ceram. Soc. doi:10.1111/j.1151-2916.1998.tb02303.x

[11] H. Huang, K. Eguchi, M. Kambara, and T. Yoshida, Ultrafast Thermal Plasma Physical Vapor Deposition of Yttria-Stabilized Zirconia for Novel Thermal Barrier Coatings, J. Therm. Spray Technol. doi:10.1361/105996306x92640

[12] A.G. Evans, D.R. Mumm, J.W. Hutchinson, G.H. Meier, F.S. Pettit, Mechanisms controlling the durability of thermal barrier coatings, Prog. Mater. Sci. doi:10.1016/s0079-6425(00)00020-7

[13] A.K. Ray, E.S. Dwarakadasa, D.K. Das, V.R. Ranganath, B. Goswami, J.K. Sahu, J.D. Whittenberger, Fatigue behavior of a thermal barrier coated superalloy at 800oC, Mater. Sci..Eng. doi:10.1016/j.msea.2006.10.035

[14] A. Rico, J. Gómez-García, C.J. Múnez, P. Poza, V. Utrilla, Mechanical properties of thermal barrier coatings after isothermal oxidation. Depth sensing indentation analysis, Surf. Coat. Technol. doi:10.1016/j.surfcoat.2009.02.035

[15] L. Xie, M.R. Dorfman, A. Cipitria, S. Paul, I.O. Golosnoy, T.W. Clyne, Properties and performance of high-purity thermal barrier coatings, J. Therm. Spray Technol. doi:10.1007/s11666-007-9079-7

[16] X. Chen, Y. Zhao, L. Gu, B. Zou, Y. Wang, X. Cao, Hot corrosion behaviour of plasma sprayed YSZ/LaMgAl11O19 composite coatings in molten sulfate–vanadate salt, Corros. Sci. doi:10.1016/j.corsci.2011.03.019

[17] J.R. Brandont, R. Taylor, Phase stability of zirconia-based thermal barrier coatings Part I. zirconia-yttria alloys, Surf.

Coat. Technol. doi:10.1016/0257-8972(91)90151-l

[18] S. Guo, Y.Kagawa, Isothermal and cycle properties of EB-PVD yttria-partially-stabilized zirconia thermal barrier coatings at 1150 and 1300oC, Ceram Int. doi:10.1016/j.ceramint.2005.10.005

[19] M. Leoni, R.L. Jones, P. Scardi, Phase stability of Scandia-yttria-stabilized zirconia TBCs. Surf. Coat. Technol. doi:10.1016/s0257-8972(98)00617-3

[20] N.A. Flecka, A.C.F. Cocksb, S. Lampenscherf, Thermal shock resistance of air plasma sprayed thermal barrier coatings, J. Eur. Ceram. Soc. doi:10.1016/j.jeurceramsoc.2014.01.002

[21] M.G. Goka, G. Goller, Microstructural characterization of GZ/CYSZ thermal barrier coatingsafter thermal shock and CMAS+hot corrosion test, J. Eur. Ceram. Soc. doi:10.1016/j.jeurceramsoc.2017.02.004

[22] E. Tzimas, H. MÜllejans, S.D. Peteves, J. Bressers and W. Stamm, Failure of thermal barrier coating systems under cyclic thermomechanical loading, Acta Mater. doi:10.1016/s1359-6454(00)00260-3

[23] D. Zhu, R.A. Miller, Investigation of thermal high cycle and low cycle fatigue mechanisms of thick thermal barrier coatings, Mater. Sci. Eng. doi:10.1016/s0921-5093(97)00852-6

[24] J. Sun, Q.G.g Fu, R.M. Yuan, K.Y. Dong, J.J. Guo, Corrosion and thermal cycling behavior of plasma sprayed thermal barrier coatings on die steel, Mater. Design. doi: 10.1016/j.matdes.2016.10.065

[25] C.H. Zhou, Q.M. Zhang, Y. Li, Thermal shock behaviors of nanostructured and microstructured thermal barrier coating on a Fe-based alloy, Surf. Coat. Technol. doi:10.1016/j.surfcoat.2012.11.074

[26] V. Kumar, K. Balasubramanian, An update on failure mechanisms of advanced thermal barrier coatings: A review, Prog. Org. Coat. doi:10.1016/j.porgcoat.2015.09.019

[27] H. Huang, C. Liu, L.Y. Ni, C.G. Zhou, Evaluation of microstructural evolution of thermal barrier coatings exposed to Na2SO4 using impedance spectroscopy, Corr. Sci. doi:10.1016/j.corsci.2010.12.023

[28] C.H. Zhou, Z.Y. Zhang, Q.M. Zhang, C.L. Lv, Y. Li, Comparison of the hot corrosion of nanostructured and microstructured thermal barrier coatings, Mater. Corr. doi:10.1002/maco.201206571

[29] R.L. Jones, Some Aspects of the Hot Corrosion of Thermal Barrier Coatings, J. Therm. Spray Technol. 1997,6,77-84. doi:10.1007/bf02646315

[30] S. Li, Z.G. Liu, J.H. Ouyang, Hot corrosion behaviour of Yb2Zr2O7 ceramic coated with V2O5 at temperatures of 600–800 OC in air, Corr. Sci. 2010,54, 3568–3572. doi:10.1016/j.corsci.2010.06.007

[31] M.H. Habibi, Li Wang, J.D. Liang, S.M. Guo, An investigation on hot corrosion behavior of YSZ-Ta2O5 in Na2SO4 + V2O5 salt at 1100oC, Corr. Sci. 2013,75,409–414. doi: 10.1016/j.corsci.2013.06.025

[32] H.F. Liu, X. Xiong, X.B. Li, Y.L Wang, Hot corrosion behavior of Sc2O3–Y2O3–ZrO2 thermal barrier coatings in presence of Na2SO4 +V2O5 molten salt, Cor. Sci. 2014,85,87–93.

[33] A. Ajaya, V.S.Raja, G.Sivakumar, S.V.Joshi, Hot corrosion behavior of solution precursor and atmospheric plasma sprayed thermal barrier coatings, Corr. Sci. 2015, 98,271–279. doi:10.1016/j.corsci.2015.05.034

[34] Z.J. Fan, K.E. Wang, X. Dong, R.J. Wang, W.Q. Duan, X.S. Mei, W.J. Wang, J.L. Cui, S. Zhang, C.Y. Xu, The role of the surface morphology and segmented cracks on the damage forms of laser re-melted thermal barrier coatings in presence of a molten salt (Na2SO4+V2O5), Corr. Sci. 2017,115,56–6[illegible] doi:10.1016/j.corsci.2016.11.011

[35] M.R. Loghman-Estarki, M. Nejati, H. Edris, R.S. Razavi, H. Jamali, A.H. Pakseresht, Evaluation of hot corrosion behavior of plasma sprayed Scandia and yttria co-stabilized nanostructured thermal barrier coatings in the presence of molten sulfate and vanadate salt, J. Eur. Ceram. Soc. 2015, 35, 693-702. doi:10.1016/j.jeurceramsoc.2014.08.029

[36] H. Jamali, R. Mozafarinia, R. Shoja-Razavi, R. Ahmadi-Pidani, Comparison of hot corrosion behaviors of plasma-sprayed nanostructured and conventional YSZ thermal barrier coatings exposure to molten vanadium pentoxide and sodium sulfate, J. Eur. Ceram. Soc. 2014, 34, 485-492. doi:10.1016/j.jeurceramsoc.2013.08.006

[37] M. Nejati, M. Rahimipour, I. Mobasherpour, Evalution of hot corrosion behavior of CSZ, CSZ/micro Al2O3 and CSZ/nano Al2O3 plasma sprayed thermal barrier coatings, Ceram. Int. 2014, 40, 4579-4590. doi:10.1016/j.ceramint.2013.08.135

[38] P. Mohan, B. Yuan, T. Patterson, V.H. Desai, and Y.H. Sohn, Degradation of Yttria-Stabilized Zirconia Thermal Barrier Coatings by Vanadium Pentoxide, Phosphorous Pentoxide, and Sodium Sulfate, J. Am. Ceram. Soc. 2007, 90, 3601-3607. doi:10.1111/j.1551-2916.2007.01941.x

[39] H. L. Tsai, P. C. Tsai, Microstructures and Properties of Laser-Glazed Plasma-Sprayed ZrO2-YO1.5/Ni-22Cr-10Al-1Y Thermal Barrier Coatings, J. Mater. Eng. Perform. 1995,4,689-696. doi:10.1007/bf02646445

[40] K. S. Shi, Z. Y. Qian, M. S. Zhuang, Microstructure and Properties of Sprayed Ceramic Coating, J. Am. Ceram. Soc. 1988,71,924-929. doi:10.1111/j.1151-2916.1988.tb07559.x

DOI: https://doi.org/10.30564/jmmr.v1i1.307